



# Urban increments of gaseous and aerosol pollutants and their sources using mobile aerosol mass spectrometry measurements

Miriam Elser<sup>1</sup>, Carlo Bozzetti<sup>1</sup>, Imad El-Haddad<sup>1</sup>, Marek Maasikmets<sup>2</sup>, Erik Teinemaa<sup>2</sup>, Rene Richter<sup>1</sup>, Robert Wolf<sup>1</sup>, Jay G. Slowik<sup>1</sup>, Urs Baltensperger<sup>1</sup>, and André S. H. Prévôt<sup>1</sup>

<sup>1</sup>Laboratory of Atmospheric Chemistry, Paul Scherrer Institute, 5232, Villigen PSI, Switzerland

<sup>2</sup>Estonian Environmental Research Centre, 10617, Tallinn, Estonia

Correspondence to: Imad El-Haddad (imad.el-haddad@psi.ch) and André S. H. Prévôt (andre.prevot@psi.ch)

Received: 14 January 2016 – Published in Atmos. Chem. Phys. Discuss.: 1 February 2016

Revised: 20 May 2016 – Accepted: 23 May 2016 – Published: 10 June 2016

**Abstract.** Air pollution is one of the main environmental concerns in urban areas, where anthropogenic emissions strongly affect air quality. This work presents the first spatially resolved detailed characterization of PM<sub>2.5</sub> (particulate matter with aerodynamic equivalent diameter  $d_{\text{aero}} \leq 2.5 \mu\text{m}$ ) in two major Estonian cities, Tallinn and Tartu. The measurements were performed in March 2014 using a mobile platform. In both cities, the non-refractory (NR)-PM<sub>2.5</sub> was characterized by a high-resolution time-of-flight aerosol mass spectrometer (HR-ToF-AMS) using a recently developed lens which increases the transmission of super-micron particles. Equivalent black carbon (eBC) and several trace gases including carbon monoxide (CO), carbon dioxide (CO<sub>2</sub>), and methane (CH<sub>4</sub>) were also measured. The chemical composition of PM<sub>2.5</sub> was found to be very similar in the two cities. Organic aerosol (OA) constituted the largest fraction, explaining on average about 52 to 60 % of the PM<sub>2.5</sub> mass. Four sources of OA were identified using positive matrix factorization (PMF): hydrocarbon-like OA (HOA, from traffic emissions), biomass burning OA (BBOA, from biomass combustion), residential influenced OA (RIOA, probably mostly from cooking processes with possible contributions from waste and coal burning), and oxygenated OA (OOA, related to secondary aerosol formation). OOA was the major OA source during nighttime, explaining on average half of the OA mass, while during daytime mobile measurements the OA was affected by point sources and dominated by the primary fraction. A strong increase in the secondary organic and inorganic components was observed during periods with transport of air masses from northern Germany, while the primary local emissions accumulated during periods with tem-

perature inversions. Mobile measurements offered the identification of different source regions within the urban areas and the assessment of the extent to which pollutants concentrations exceeded regional background levels (urban increments). HOA, eBC, CO<sub>2</sub>, and CO showed stronger enhancements on busy roads during the morning and evening traffic rush hours; BBOA had its maximum enhancement in the residential areas during the evening hours and RIOA was enhanced in both the city center (emissions from restaurants) and in the residential areas (emissions from residential cooking). In contrast, secondary components (OOA, sulfate (SO<sub>4</sub>), nitrate (NO<sub>3</sub>), ammonium (NH<sub>4</sub>), and chloride (Cl)) had very homogeneous distributions in time and space. We were able to determine a total PM<sub>2.5</sub> urban increment in Tartu of  $6.0 \mu\text{g m}^{-3}$  over a regional background concentration of  $4.0 \mu\text{g m}^{-3}$  (i.e., a factor of 2.5 increase). Traffic exhaust emissions were identified as the most important source of this increase, with eBC and HOA explaining on average 53.3 and 20.5 % of the total increment, respectively.

## 1 Introduction

Atmospheric particulate matter (PM) plays a central role in many environmental processes through its influence on climate (radiative forcing; Myhre et al., 2013), the hydrological cycle (Ramanathan et al., 2001), and its adverse effects on health (Pope and Dockery, 2006). Major attention has been devoted to the study of the PM<sub>2.5</sub> fraction (particulate matter with an aerodynamic equivalent diameter  $d_{\text{aero}} \leq 2.5 \mu\text{m}$ ), which has been linked to increased lung cancer rates (Hu and

Jiang, 2014), acute bronchitis and asthma (Gao et al., 2015), and mortality (Dockery et al., 1993; Laden et al., 2006). Atmospheric particles can be classified as primary or secondary aerosols according to their formation processes. Primary particles are directly emitted, while secondary aerosols are formed from gas-phase precursors following chemical transformation in the atmosphere. Aerosols can be further classified in terms of their emission sources as natural sources (e.g., volcanic eruptions, wildfires, sea salt, dust, or biogenic emissions from plants) or anthropogenic sources (mostly from combustion processes, e.g., traffic and residential wood combustion).

Due to enhanced contributions of anthropogenic sources, air quality is commonly lower in urban areas compared to rural or suburban locations (Putaud et al., 2004). In Europe, annual average  $\text{PM}_{2.5}$  mass concentrations in urban areas commonly vary between a few  $\mu\text{g m}^{-3}$  up to  $35 \mu\text{g m}^{-3}$  (Putaud et al., 2010). The predominance of specific aerosol sources (e.g., residential, traffic, industry) or the implementation of new technologies (e.g., car fleet, heating systems) may strongly influence the levels and physicochemical characteristics of the pollutants in these locations. Moreover, certain orographic features and stagnant meteorological conditions may induce the accumulation of local pollutants (Putaud et al., 2004; Carbone et al., 2010; Squizzato et al., 2012). Likewise, long-range transport of continental air masses has been shown to influence PM in different urban areas in Europe (Niemi et al., 2009; Baker, 2010; Salvador et al., 2013; Beekmann et al., 2015; Di Gilio et al., 2015; Ulevicius et al., 2016). While the PM levels and physicochemical properties of the particles are well characterized in Western Europe, data are scarce in Eastern European cities, especially in the Baltic region, hindering air quality assessment and quantification of the main aerosol sources.

In contrast to conventional stationary measurements, mobile measurements (including zeppelin, aircraft, and ground measurements) are suited for pollutant mapping, chasing of mobile sources or measurements in emission plumes, etc. Ground-based measurements by mobile platforms have been successfully performed in the last years to measure particles and trace gases from real-world traffic emissions (Bukowiecki et al., 2002, 2003; Pirjola et al., 2004, 2006, 2012; Kwak et al., 2014; Kyung Hwan et al., 2015) and from wood burning emissions (Pirjola et al., 2015). More recently, aerosol mass spectrometers (AMSs) have been deployed in mobile laboratories in order to determine the physical and chemical properties of submicron aerosols ( $\text{PM}_1$ , particulate matter with aerodynamic equivalent diameter  $d_{\text{aero}} \leq 1 \mu\text{m}$ ) in urban environments like Zurich (Mohr et al., 2011), Paris (von der Weiden-Reinmüller et al., 2014a, b), or Barcelona (Mohr et al., 2015). Moreover, a newly developed inlet for the AMS has been used to measure the chemical composition of the non-refractory (NR)- $\text{PM}_{2.5}$  fraction in the Po Valley (Wolf et al., 2015).

In this work we present the first detailed in situ mass spectrometric measurements of air pollutants in the two biggest cities in Estonia (Tallinn and Tartu). The measurements were performed using the Paul Scherrer Institute (PSI) mobile laboratory (Bukowiecki et al., 2002; Mohr et al., 2011; Wolf et al., 2015). The use of a high-resolution time-of-flight aerosol mass spectrometer (HR-ToF-AMS) with a novel  $\text{PM}_{2.5}$  lens offered a detailed characterization of the NR- $\text{PM}_{2.5}$  fraction in the measurement areas. The spatial distributions of the sources of organic aerosols (OA), inorganic aerosols (nitrate ( $\text{NO}_3$ ), sulfate ( $\text{SO}_4$ ), ammonium ( $\text{NH}_4$ ), and chloride ( $\text{Cl}$ )), equivalent black carbon (eBC), and some of the major gas-phase components (carbon monoxide (CO), carbon dioxide ( $\text{CO}_2$ ), and methane ( $\text{CH}_4$ )) were determined in the urban areas. Such analyses allowed for the calculation of regional background and urban concentrations of the different gas- and particle-phase components and provided direct insights into the spatial resolution of local emissions and their impact on the air quality in different city areas. Long-range transport of pollutants and accumulation events as well as their effect on the particle- and gas-phase mass concentrations will also be discussed.

## 2 Methodologies

### 2.1 Measurement campaign

The measurements were performed in the two biggest cities in Estonia. Tallinn, the capital and the largest city of Estonia, has a population of 413 000 inhabitants (Statistical Database, 2015) and occupies an area of  $158.3 \text{ km}^2$ . Located on the northern coast of the country, Tallinn has some of the biggest ports in the Baltic Sea. Among them, the old city harbor is one of the busiest passenger harbors in the region. Tartu, with an area of  $38.8 \text{ km}^2$  and more than 97 000 inhabitants in 2015 (Statistical Database, 2015), is the second largest city in Estonia. The city is situated in the center of southern Estonia, in the post-glacial valley of the Emajõgi River, which influences the local meteorological conditions and favors the accumulation of local pollutants under frequent temperature inversions. Previous studies identified traffic emissions and residential heating as the major sources of air pollution in these two cities (Urb et al., 2005; Orru et al., 2011). An older vehicle fleet, the limited network capacity of the city streets (which generates congestions during rush hours), and the extensive use of studded tires have been reported to strongly enhance the signal of traffic emissions in the city center and major roads (Urb et al., 2005; Orru et al., 2011). Residential heating includes extensive use of inefficient wood and coal stoves with low stacks in both cities. In this regard, a detailed modeling study performed in Tallinn and Tartu (Orru et al., 2011) revealed that the city centers and the neighborhoods with local heating are exposed to much higher average  $\text{PM}_{2.5}$  concentrations compared to other areas of the cities.

The measurements took place from 10 to 17 March 2014 in Tartu and from 25 March to 1 April 2014 in Tallinn. Emission maps including residential wood combustion and industrial sources and the traffic emission rates in the major streets of the two cities are reported in Fig. S1 in the Supplement. The driving routes were chosen in order to cover heavily trafficked roads, residential areas, and background sites with little local emissions. In Tallinn, streets close to the old town harbor were also included in the route. To obtain statistically significant spatial distributions of the major pollutants, 25 loops were performed at each location throughout the measurement periods at different times of the day. The average loop duration was about 72 min in Tartu and 112 min in Tallinn. Stationary measurements were typically performed overnight at a gasoline station in Tartu (influenced by city center and residential emissions) and at the Estonian Environmental Research Centre (EERC) in Tallinn (a background site). Meteorological data were recorded on a meteorological tower in K ilitse (around 10 km southeast from Tartu) and in the Tartu and Tallinn Zoo meteorological stations. The most relevant parameters (including wind direction and speed, temperature, and precipitation) are reported in Fig. S2 in the Supplement.

## 2.2 Mobile laboratory setup

A schematic of the instrumental setup in the PSI mobile platform is shown in Fig. S3. The main inlet of the mobile platform was kept at a constant velocity of  $\sim 11 \text{ m s}^{-1}$  for isokinetic sampling during driving conditions, assuming an average velocity in the city of  $\sim 40 \text{ km h}^{-1}$ . Two different inlet lines connected the main inlet to the aerosol and gas-phase instrumentation. The size cutoff of the inlet system was estimated to be around  $5 \mu\text{m}$ . The deployed instruments, measured parameters and their time resolution are listed in Table 1. All parameters were determined with high time resolution (between 1 and 25 s), critical for the identification of source regions using a mobile platform.

An HR-ToF-AMS (Aerodyne Research Inc.) was deployed to measure the chemical composition of the NR-PM<sub>2.5</sub> aerosol, including NO<sub>3</sub>, SO<sub>4</sub>, NH<sub>4</sub>, Cl, and OA. For this work, the AMS was equipped with a recently developed aerodynamic lens which extends the measured particle size to the PM<sub>2.5</sub> fraction (in contrast to the conventional PM<sub>1</sub> lens). The PM<sub>2.5</sub> lens efficiently transmits particles between 80 nm and up to at least  $3 \mu\text{m}$  and has been well characterized by Williams et al. (2013) and tested in previous chamber and ambient studies (Wolf et al., 2015; Elser et al., 2016). The operating principle of the instrument can be found elsewhere (DeCarlo et al., 2006). A nafion drier (Perma Pure MD-110) was set before the AMS inlet in order to dry the ambient particles and reduce uncertainties in the bounce-related collection efficiency (CE<sub>b</sub>) and possible transmission losses of large particles at high relative humidity.

A seven-wavelength Aethalometer (Magee Scientific, model AE33) was used to measure the aerosol light absorption and to determine the eBC concentrations. The measurement at seven different wavelengths (370, 470, 520, 590, 660, 880, and 950 nm) covers the range between ultraviolet and infrared and allows for the source apportionment of different eBC fractions (Sandradewi et al., 2008; Zotter et al., 2015). Moreover, the dual spot measurement method automatically corrects for the loading effect and provides a real-time calculation of the loading compensation parameter (Drinovec et al., 2015).

The gas concentrations were measured by a Picarro-G2301 CO / CO<sub>2</sub> / CH<sub>4</sub> analyzer and a Licor-6262 CO monitor. In addition, some important parameters for mobile measurements (GPS, temperature, relative humidity, and solar radiation) were also measured continuously.

## 2.3 AMS data analysis

AMS data were analyzed in Igor Pro 6.3 (WaveMetrics) using the standard ToF-AMS Data Analysis toolkit (SQUIRREL version 1.53G and PIKA version 1.12G). Based on standard NH<sub>4</sub>NO<sub>3</sub> calibrations, the ionization efficiency (defined as ions detected per molecules vaporized) was determined to be  $5.08 \times 10^{-8}$  (average of five calibrations during the full measurement period). Standard relative ionization efficiencies (RIEs) were used for nitrate, chloride, and organics (RIE = 1.1, 1.3, and 1.4, respectively) and experimentally determined for sulfate and ammonium (RIE = 1.11 and 4.29, respectively). A composition-dependent CE algorithm by Middlebrook et al. (2012) was used in the calculation of ambient mass concentrations (Middlebrook et al., 2012).

## 2.4 Source apportionment techniques

### 2.4.1 OA source apportionment

To identify and quantify the major sources of OA in the different measurement areas, positive matrix factorization (PMF; Paatero and Tapper, 1994) was applied to the time resolved AMS data (see Table 1). The analysis was performed using the multilinear engine tool (ME-2; Paatero, 1997) implemented in the Source Finder interface (SoFi; Canonaco et al., 2013) coded in Igor Wavemetrics.

PMF is a bilinear unmixing algorithm which, as defined in Eq. (1), allows the representation of a two-dimensional matrix of measured data (**X**) as a linear combination of a given number of static factors profiles (**F**) and their corresponding time series (**G**). The matrix **E** in Eq. (1) contains the model residuals. The model uses a least squares approach to iteratively minimize the object function *Q* described in Eq. (2):

**Table 1.** Instrument list, measured components, and time resolution of each measurement.

	Instrument list	Measured components	Time resolution
Aerosols	HR-ToF-AMS	Size resolved chemical composition of NR-PM <sub>2.5</sub>	25 s
	Aethalometer	eBC (absorption coefficient at 7λ)	1 s
Gases	CO <sub>2</sub> Picarro	CO <sub>2</sub> , CO, CH <sub>4</sub> , H <sub>2</sub> O	1 s
	CO <sub>2</sub> Licor	CO <sub>2</sub> , H <sub>2</sub> O	1 s
Others	GPS, temperature, relative humidity, and solar radiation		2 s

$$\mathbf{X} = \mathbf{GF} + \mathbf{E} \quad (1)$$

$$Q = \sum_{i=1}^m \sum_{j=1}^n \left( \frac{e_{ij}}{\sigma_{ij}} \right)^2, \quad (2)$$

where  $e_{ij}$  are the elements of the error matrix ( $\mathbf{E}$ ) and  $\sigma_{ij}$  are the respective uncertainties of  $\mathbf{X}$ .

In our case, the model input are the data and error matrices of OA mass spectra, where the rows represent the time series (62 665 points, with steps of 25 s) and the columns contain the fits to the high-resolution data (292 ions). The organic mass obtained from the high-resolution fits (up to  $m/z$  115) agrees with the mass calculated from the unit mass resolution integration (up to  $m/z$  737) within  $\pm 5\%$ . The initial error values were calculated with the HR-AMS data analysis software PIKA. A minimum error corresponding to the measurement of a single ion was applied (Ulbrich et al., 2009). All variables with signal-to-noise ratio (SNR) lower than 0.2 were removed and the variables with SNR between 0.2 and 2 were down-weighted by increasing their error by a factor of 3 (Paatero and Hopke, 2003). Moreover, all variables directly calculated from the CO<sub>2</sub><sup>+</sup> fragment using the organic fragmentation table (i.e., O<sup>+</sup>, HO<sup>+</sup>, H<sub>2</sub>O<sup>+</sup>, and CO<sup>+</sup>) (Allan et al., 2004) were excluded from the PMF analysis to appropriately weight the variability of the CO<sub>2</sub><sup>+</sup>; these ions were reinserted post-analysis.

The possibility of local minima in the solution space and the uncertainty of the PMF solution were investigated by means of bootstrap analysis. This statistical method is based on the creation of replicate datasets resulting from the perturbation of the original data by resampling. In each replicate, some randomly chosen rows of the original matrix are present several times, while other rows are removed (Paatero et al., 2014), such that the dimension of the data matrix is kept constant. This resulted in about 64 % of the original points being used in each replicate. PMF was applied to 100 different replicates and the variations among these results were used to estimate the uncertainty of the initial PMF solution. Note that each bootstrap run is started from a different initialization point; thus, this methodology inherently includes the investigation of the classic seed variability. All

convergent solutions were found to be consistent, suggesting that the solution is robust.

The results presented in this section were obtained by merging the measurements from the two measurement locations, as no major changes were observed if the source apportionment was performed for the individual cities.

## 2.4.2 eBC source apportionment

The Aethalometer measurements can be used to separate eBC from wood burning (eBC<sub>wb</sub>) and from traffic (eBC<sub>tr</sub>), by taking advantage of the spectral dependence of absorption, as described by the Ångström exponent (Ångström, 1929). Specifically, the enhanced absorption of wood burning particles in the ultraviolet and visible wavelengths region (370–520 nm) relative to that of traffic particles is used to separate the contributions of the two fractions. This method is described in detail in Sandradewi et al. (2008) and has been successfully applied at many locations across Europe (Favez et al., 2010; Herich et al., 2011; Sciare et al., 2011; Crilley et al., 2015). For a proper separation of the eBC fractions, the Aethalometer data were averaged to 30 min in order to increase the SNR. Thus, the obtained fractions eBC<sub>wb</sub> and eBC<sub>tr</sub> could only be used for the correlations with the external tracers, but their spatial distributions could not be explored. The absorption Ångström exponent was calculated using the absorption measured at 470 and 950 nm and Ångström exponents of 0.9 and 1.7 were used for traffic and wood burning, respectively. More details on the choice of the wavelengths and Ångström exponents are presented in the Supplement.

## 3 Results and discussion

### 3.1 Pollutant concentrations and temporal variability

The temporal variation of all measured gas- and particle-phase components is shown in Fig. 1a. The type of measurement is indicated by different background colors (transparent for stationary measurements and orange for mobile measurements). The measurement period included three distinct meteorological periods of transport of polluted air masses

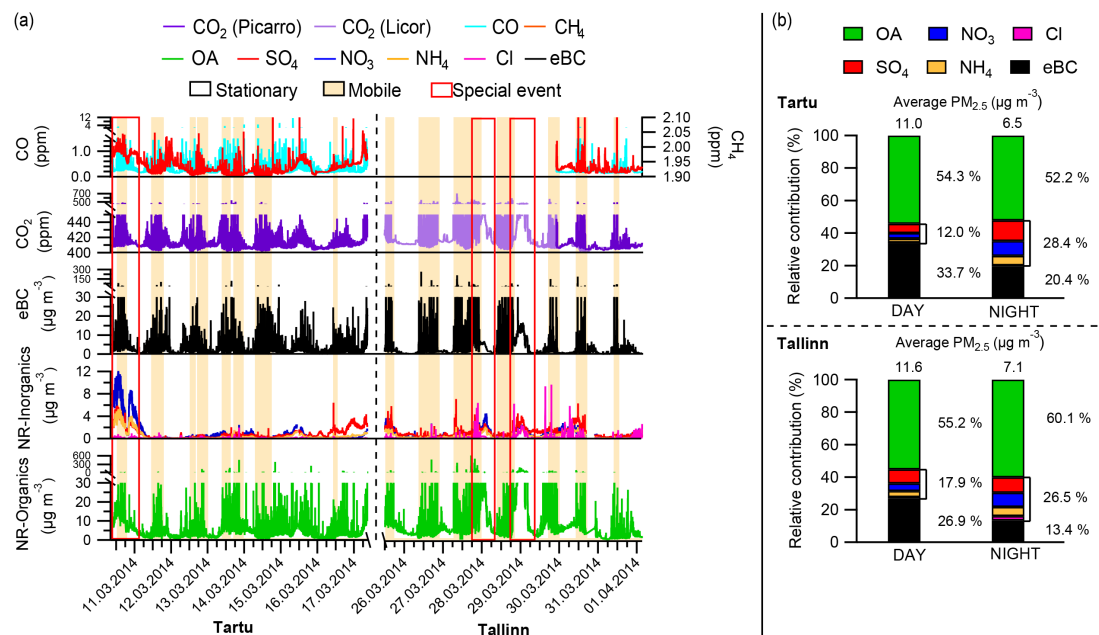


**Figure 1.** (a) Temporal evolution of all gas- and particle-phase measured components over the full measurement period; (b) average PM<sub>2.5</sub> (NR-PM<sub>2.5</sub> plus eBC) mass concentration and chemical composition for the measurements in Tartu (top panel) and Tallinn (bottom panel), with day- and nighttime distinction. Note: special events were excluded.

and accumulation of local emissions. These periods are referred to as special events (indicated by a red frame) and will be treated separately and discussed in detail in Sect. 3.4. While the AMS and Aethalometer were running almost continuously during the entire measurement period, there is a small gap in the CO<sub>2</sub>, CO, and CH<sub>4</sub> data due to an instrument malfunction. Over the full measurement period, the average mass concentration of PM<sub>2.5</sub> (NR-PM<sub>2.5</sub> plus eBC) was 12.3 µg m<sup>-3</sup>. In the gas-phase, average concentrations of 414.1 ppm of CO<sub>2</sub>, 0.24 ppm of CO, and 1.92 ppm of CH<sub>4</sub> were measured. In contrast to these relatively low average values, extremely high concentrations were often recorded during the mobile measurements due to local emissions from point sources (around 50 spikes with PM<sub>2.5</sub> mass concentration exceeding 100 µg m<sup>-3</sup>). Such intermittent pollution plumes (expected in some areas in a city) cannot be detected from stationary measurements at an urban background site but may be associated with negative health impacts. As shown in Fig. 1b, neglecting the periods defined as special events, the PM<sub>2.5</sub> average concentrations and relative contributions of the particle-phase species were very similar at the two locations. If we compare daytime (07:00 to 19:00, local time (LT)) and nighttime (19:00 to 07:00 LT) measurements, in both cities the average PM<sub>2.5</sub> was higher during the day (11.0 µg m<sup>-3</sup> in Tartu and 11.6 µg m<sup>-3</sup> in Tallinn) than during the night (6.5 µg m<sup>-3</sup> in Tartu and 7.1 µg m<sup>-3</sup> in Tallinn) despite the development of the boundary layer and increased dilution during daytime. OA constituted in all cases the largest mass fraction, explaining on average 52.2

and 54.3 % of the PM<sub>2.5</sub> mass in Tartu (during night- and daytime, respectively) and 55.2 and 60.1 % in Tallinn (during day- and nighttime, respectively). Primary emissions of eBC contributed on average 20.4 and 33.7 % in Tartu (during day- and nighttime respectively) and 13.4 and 26.9 % in Tallinn (during day- and nighttime, respectively), constituting a substantially higher fraction than at other European locations (Putaud et al., 2010). The remaining mass, 12 to 28 %, was related to secondary inorganic species, mostly ammonium sulfate and nitrate. These species were found to be neutralized within the uncertainties (ratio of NH<sub>4</sub> expected from an ion balance to NH<sub>4</sub> measured of 1.05, with  $R^2 = 0.95$ ). During nighttime a decrease in the relative contribution of eBC was observed in favor of an enhanced contribution of the inorganic species.

### 3.2 Sources of OA

To properly represent the temporal variations of the OA, four factors were required: hydrocarbon-like OA (HOA), biomass burning OA (BBOA), residential influenced OA (RIOA), and oxygenated OA (OOA). The mass spectra of these factors are reported in Fig. 2. HOA is a primary source related to traffic emissions and its mass spectrum is characterized by the presence of alkyl fragment signatures (Ng et al., 2011), with prominent contributions of non-oxygenated species at  $m/z$  43 (C<sub>3</sub>H<sub>7</sub><sup>+</sup>),  $m/z$  55 (C<sub>4</sub>H<sub>7</sub><sup>+</sup>), and  $m/z$  57 (C<sub>4</sub>H<sub>9</sub><sup>+</sup>). As shown in Fig. S4, a fairly good correlation is found between HOA and eBC<sub>tr</sub> ( $R^2 = 0.4$ ). Moreover, the ratio of HOA to eBC<sub>tr</sub> was 0.5, which is in good agreement with

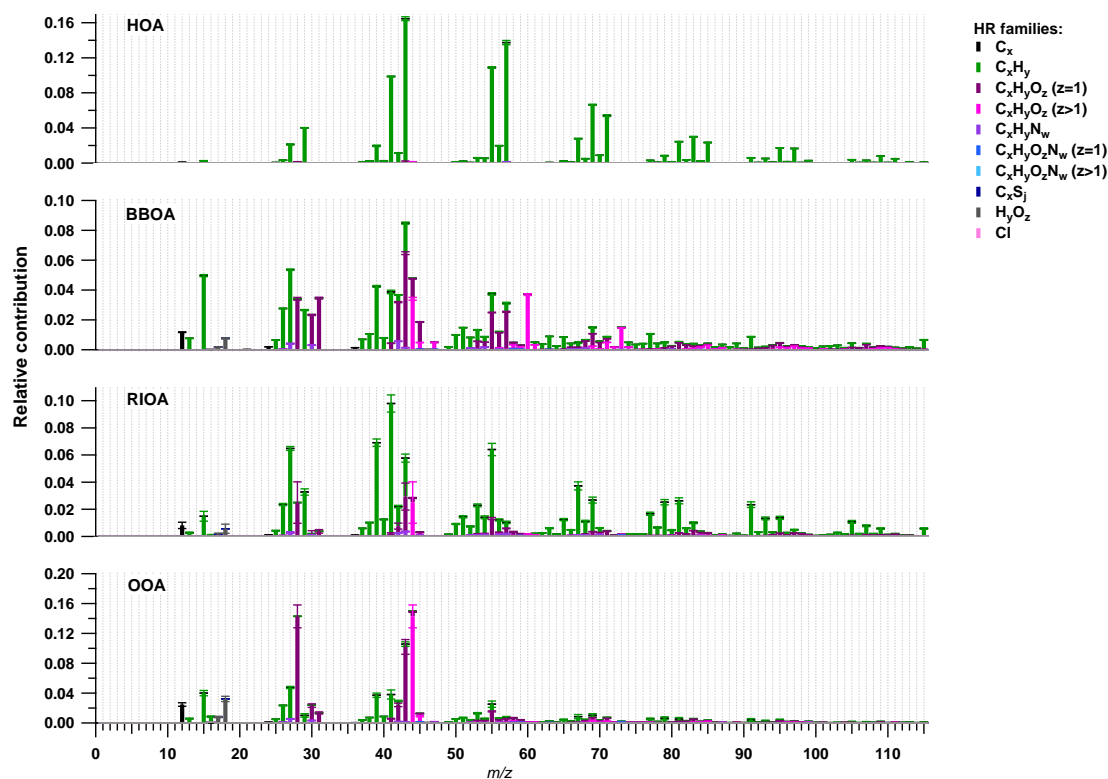


**Figure 2.** Mass spectra of the four OA sources identified with PMF. From top to bottom: hydrocarbon-like OA (HOA), biomass burning OA (BBOA), residential influenced OA (RIOA), and oxygenated OA (OOA). Error bars indicate the standard deviation among 100 bootstrap runs.

**Table 2.** Correlation coefficients ( $R^2$ ) between the OA profiles from the four-factor solution and literature profiles. The different nomenclatures used in the literature for the OOA factors have been homogenized to a semi-volatile OOA (SVOOA) and a low-volatility OOA (LVOOA).

$R^2$	Aiken et al. (2009)	Mohr et al. (2012)	Setyan et al. (2012)	Crippa et al. (2013b)
HOA-HOA	0.82	0.96	0.72	0.78
BBOA-BBOA	0.86	0.68	–	–
RIOA-COA	–	0.83	–	0.81
OOA-SVOOA	0.96	0.72	0.90	0.71
OOA-LVOOA	0.91	0.93	0.94	0.96

previous European studies (El Haddad et al., 2013, and references therein). BBOA is associated with domestic heating and/or agricultural biomass burning activities and shows characteristic high contributions of the oxygenated hydrocarbons at  $m/z$  60 ( $C_2H_4O_2^+$ ) and  $m/z$  73 ( $C_3H_5O_2^+$ ), which are known fragments from anhydrous sugars (Alfarra et al., 2007). BBOA correlates fairly well with  $eBC_{wb}$  ( $R^2 = 0.4$ ), and the ratio of BBOA to  $eBC_{wb}$  was 4.0 (Fig. S4), which within the method uncertainties is consistent with previously reported values (Crippa et al., 2013a). The ratio BBOA to  $eBC_{wb}$  was found to be very sensitive to the chosen Ångström exponent for traffic, and it increased to 4.8 when a slightly higher Ångström exponent (i.e., 1.0 instead of 0.9)

was considered for traffic. RIOA is a hydrocarbon-rich factor that was required for a reasonable explanation of the variability in the data. Due to its increase in the residential areas, this factor was associated with residential emissions. Given its strong correlation ( $R^2 = 0.9$ ) with cooking markers such as the fragment ion  $C_6H_{10}O^+$  at  $m/z$  98 (Sun et al., 2011; Crippa et al., 2013b), we expect that a great part of this factor is related to cooking emissions (see Fig. S4). Moreover, as in previously reported cooking spectra (Mohr et al., 2012), the RIOA mass spectrum shows a higher  $m/z$  55 to  $m/z$  57 ratio than HOA. However, in the absence of diurnal trends due to the driving conditions, the separation of cooking emissions from other residential emissions (such as domestic coal



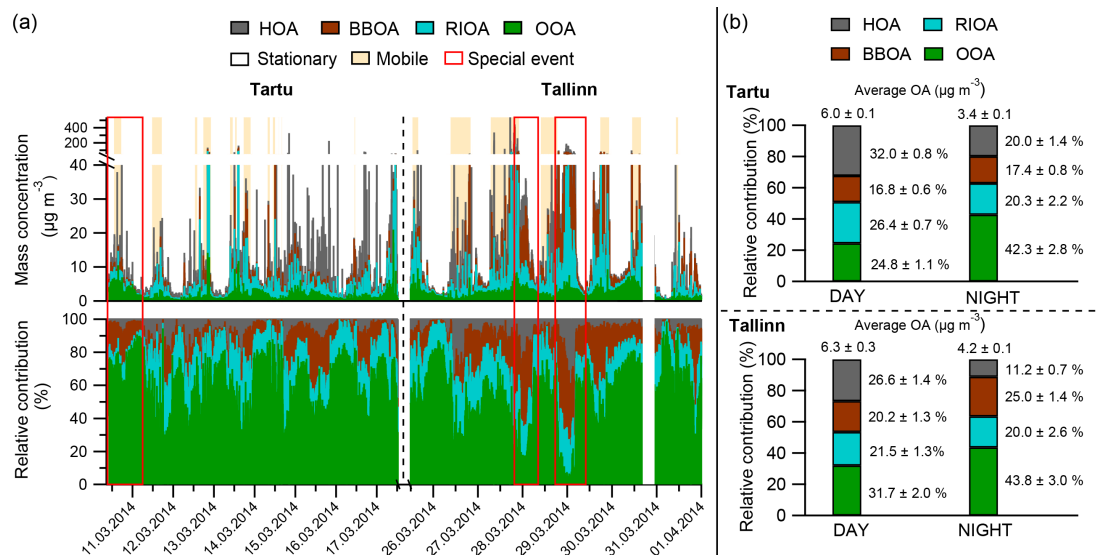


**Figure 3.** (a) Temporal evolution of the absolute mass (top panel) and relative contributions (bottom panel) of the four OA sources over the full measurement period; (b) average OA mass concentrations and relative contributions of the OA sources for the measurements in Tartu (top panel) and Tallinn (bottom panel), with day- and nighttime distinction. Errors indicate the standard deviation among 100 bootstrap runs. Note: special events were excluded.

and waste burning) was not possible. OOA is associated with aged emissions and secondary organic aerosol formation, and its profile is characterized by a very high  $m/z$  44 ( $\text{CO}_2^+$ ). In general, OOA increases simultaneously with the secondary species (especially  $\text{NO}_3$ ), but the ratio among these components changes during special events (Fig. S4).

Some important diagnostic parameters of the source apportionment (including  $Q/Q_{\text{exp}}$ , factor–marker correlation, and time series and profile residuals for solutions with different number of factors) are reported in Fig. S5. The correlation coefficients ( $R^2$ ) between factors and markers significantly increase when a fourth factor is included but are not improved when a fifth factor is added. The addition of the fourth factor, which enabled the extraction of RIOA, allows explaining additional structures in the residuals’ time series and unsaturated fragments in the residuals mass spectrum. Including a fifth factor also improves the model mathematical quality by additionally explaining  $\text{C}_x\text{H}_y\text{N}_w$  and biomass burning (at  $m/z$  60 and 73) related fragments. The additionally extracted factor in the five-factor solution, referred to as “unknown”, has elevated contributions from oxygenated fragments often related to secondary organic aerosols ( $m/z$  44) and BBOA ( $m/z$  60 and 73) but also a time series that unambiguously relates this factor to a spatially variable primary emission source. In effect, the majority (62 %) of this factor contribution arises from a split in the BBOA factor from the four-factor solution (the rest comes from the residuals and the OOA). Moreover, the sum of the contributions of the “unknown” factor and the BBOA from the five-factor solution matches the BBOA contributions from the four-factor solution ( $R^2 = 0.97$  and slope = 1.15 as shown in Fig. S6).

This split in the BBOA is very likely a direct consequence of the variable nature of this combustion source, but the two BBOA-like factors extracted in the five-factor solution could not be related to different emission processes. Furthermore, the addition of this factor did not affect the spectral profiles and time series of the other factors and their correlations with their respective markers and did not aid the interpretation of the data. Therefore, we considered the four-factor solution as an optimal representation of our data. Table 2 contains the correlation coefficients ( $R^2$ ) between the OA profiles from the four-factor solution and available literature profiles (Aiken et al., 2009; Mohr et al., 2012; Setyan et al., 2012; Crippa et al., 2013b). The high correlations obtained in all cases support the use of a four-factor solution and strengthen the link between the RIOA and cooking emissions ( $R^2$  of about 0.8 between RIOA and cooking tracer).

Figure 3a represents the time series of the absolute mass (top panel) and relative contributions (bottom panel) of the retrieved OA sources for the two measurement locations. The variability of these time series over 100 bootstrap runs was relatively low, as shown in Fig. S9. In both cities, the three primary sources (HOA, BBOA, and RIOA) exhibit a very spiky temporal behavior, while the secondary source (OOA) is characterized by a relatively smooth time series. Figure 3b reports the averaged total OA mass and relative contributions of the OA sources during the measurements in Tartu (top panel) and Tallinn (bottom panel). The reported errors (which correspond to the standard deviation among 100 bootstrap runs) are an indication of the high stability of the solution. Overall, the relative errors vary between 3 and 7 %, except for the RIOA, which shows slightly higher variability dur-

ing nighttime (relative error of 11 % in Tartu and 13 % in Tallinn). Similarly to the total  $\text{PM}_{2.5}$  mass and as reported in Fig. 3b, neglecting the special events, a strong daily cycle can be observed in the total OA mass, with higher concentrations during daytime ( $6.0$  and  $6.3 \mu\text{g m}^{-3}$  in Tartu and Tallinn, respectively) than during nighttime ( $3.4$  and  $4.2 \mu\text{g m}^{-3}$  in Tartu and Tallinn, respectively). This difference is mostly driven by the increase of primary aerosol emissions (HOA, BBOA, and RIOA) during the day. This structure is observed independently of the nature of the measurements (stationary or mobile), indicating that except for the periods where emissions from point sources are sampled, the OA concentrations and sources are rather homogeneous across the sampling area. In terms of relative contribution, OOA is dominant during nighttime, explaining on average between 42 and 44 % of the OA mass in Tartu and Tallinn, respectively. The relative contribution of HOA to total OA mass is higher during daytime (32 % in Tartu and 27 % in Tallinn) than during nighttime (20 % in Tartu and 11 % in Tallinn). RIOA is also enhanced during daytime in Tartu (27 % compared to 20 % during nighttime) and has similar relative contributions for day- and nighttime in Tallinn (20 and 22 %, respectively). In contrast, BBOA shows similar relative contributions for day- and nighttime in Tartu (representing about 17 % of the OA mass) and slightly lower contributions during daytime in Tallinn (20 % during daytime and 25 % at nighttime).

### 3.3 Spatial distributions, regional background, and urban increments

The average spatial distributions of the four OA sources,  $\text{SO}_4$ ,  $\text{NO}_3$ , eBC,  $\text{CO}_2$ , and CO are represented in Figs. 4 and 5 for Tartu and Tallinn, respectively. The spatial distributions of the additionally measured gas and particle components are reported in Figs. S10 and S11. All loops for which all the instruments were running (except  $\text{CO}_2$ , CO, and  $\text{CH}_4$  in Tallinn) were averaged on a grid with grid cells of  $250 \text{ m}^2$ . In order to get comparable distributions from different days of measurements, the fifth percentile (P05) was subtracted from each single loop for all components. The subtraction of P05 was found to be optimal to decrease the variability among different loops enough to make them comparable. However, as it will be discussed in the following, P05 was not always sufficient to capture the regional background concentrations. The color scales in Figs. 4 and 5 represent the averaged enhancement over the background concentrations of each source/species. For a better visualization, the maximum of the color scale was set at the 75th percentile (P75) for  $\text{SO}_4$ ,  $\text{NO}_3$ , eBC,  $\text{CO}_2$ , and CO. Moreover, the highest 75th percentile among all OA sources (i.e.,  $1.2 \mu\text{g m}^{-3}$  in Tartu and  $2.4 \mu\text{g m}^{-3}$  in Tallinn) was used as a maximum for the four OA sources in order to facilitate the comparison among them. Lastly, the sizes of the points represent the number of measurement points that were averaged in each case. The correlation coefficients ( $R^2$ ) between the spatial distributions of

all sources and components are reported in Table S1 in the Supplement.

Longitude profiles of the enhancements of all considered components were obtained for Tartu by averaging the calculated enhancements in longitude bins (using the same grid of  $250 \text{ m}^2$  as above). These results are shown in Fig. 6 (averages and standard deviation among all loops), Fig. S12 (median and first and third quartiles), and Fig. S13 (separation of all loops into time bins of 2 h). The longitude profiles in Figs. 6 and S12 allowed for the calculation of regional background concentrations and urban increments, as defined by Lenschow et al. (2001) and reported in Table 3. The urban concentrations, which are given by the sum of the regional background and the urban increment, represent a mix of urban background and curbside locations. While the averaged profiles take into account the effects of the measured point sources in the urban area (mostly traffic and residential emissions), the use of the median profiles is expected to represent more selectively the urban background concentrations. We note that the influence of curbside increments may not be completely removed when using median increments (e.g., accumulation of traffic emissions due to street canyon effects), and therefore these increments might be biased high and should be regarded as our highest estimates of urban background concentrations. In the following we will present the results related to the average profiles, followed by the results from the median profiles reported in parenthesis. In all cases, the longitude profiles were fitted using sigmoid functions (black curves). In order to have a constant averaging city area, the fitting limits (indicated with blue and pink arrows) and the  $x$  value of the sigmoid's midpoint ( $X_0$ ) were determined from the fit of the total  $\text{PM}_{2.5}$  mass (NR- $\text{PM}_{2.5}$  plus eBC) and imposed to all other components. In most cases the base of the sigmoid function is slightly above zero. This indicates that the subtracted P05 did not represent the full regional background, which is therefore given by the sum of the average P05 and the base of the sigmoid function. Note that the initial subtraction of P05 would not be necessary if the longitudinal profile of each single loop could be fitted. However, this is not possible due to the high concentration variability within each single loop. A sensitivity analysis was performed by using P10 instead of P05 and no major changes were observed in the final results. As shown by the wind rose in Fig. 4b, during the drives in Tartu the wind was predominantly from the west. However, the background concentrations measured at the eastern side of the loop do not seem to be affected by the transport of pollutants from the urban area, as the base values obtained for the eastern side are equal or lower than those from the western side (see Table 3). As the differences between the west and east fits are in most cases rather low, we use the west–east averages of the base values to calculate the urban increments concentrations in Table 3.

In Tartu, the three primary OA sources (HOA, BBOA, and RIOA) show a clear enhancement in the city center com-



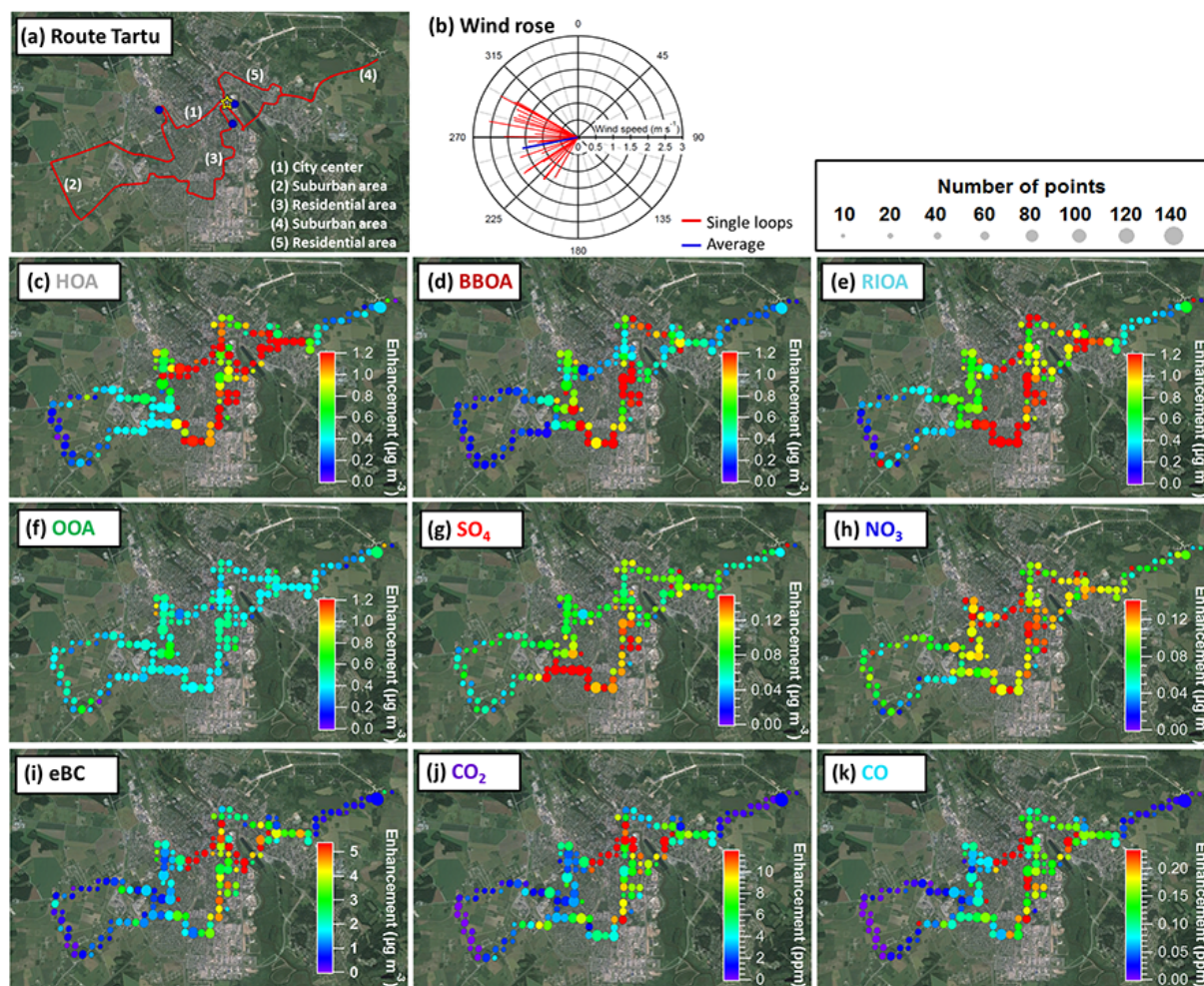


**Figure 4.** (a) Driving route in Tartu: the red trace represents the GPS data, the yellow star the stationary measurements location, and the blue dots the monitoring stations of the Estonian Environmental Research Institute (EERC); (b) wind conditions during the mobile measurements in Tartu: red traces represent the wind direction and speed for the single loops and the average of all loops is represented in blue; (c to k) average spatial distributions of all identified OA sources (panels c to f) and other measured components (panels g to k) in Tartu. The color scales represent enhancement over the background concentrations; the maximum of the color scales is fixed to the 75th percentile of the average enhancement of each component in panels (g) to (k) and to the highest 75th percentile among all OA sources in panels (c) to (f). The sizes of the points represent the number of points that were averaged in each case.

pared to the suburban areas (Figs. 6 and S12). Moreover, different source regions (see Fig. 4c–f) and emission times (see Fig. S13) can be distinguished inside the urban area. For example, maximum HOA concentrations are observed on highly congested roads, especially at sites under stop-and-go conditions and show a maximum enhancement in the morning and evening traffic rush hours (07:00 to 09:00 and 15:00 to 17:00 LT). The spatial distributions of the eBC, CO<sub>2</sub>, and CO (Fig. 4i–k) are consistent with that of HOA ( $R^2$  of 0.61, 0.59, and 0.58, respectively), which indicates that these species originate mostly from traffic. BBOA is strongly enhanced in the residential areas, consistent with the distribution of residential wood combustion sources shown in Fig. S1. The maximum BBOA enhancement is seen in the

evening hours (15:00 to 21:00 LT) when domestic heating is more active. RIOA shows enhanced contributions in both, the residential areas (probably related to domestic cooking emissions) and the major roads in the city center (probably related to cooking emissions from restaurants). The maximum enhancement of RIOA is also seen in the evening hours (15:00 to 19:00 LT), during and after the evening maximum of HOA. In contrast, OOA (Fig. 4f) and the other secondary species (SO<sub>4</sub>, NO<sub>3</sub>, NH<sub>4</sub>, and Cl; see Figs. 4g–h and S10) show very homogeneous spatial distribution over the whole measurement area (as expected from their secondary nature), and no clear dependence on the time of the day can be seen for the OOA (Fig. S13). Although slight enhancements are observed in these components close to residential areas (OOA



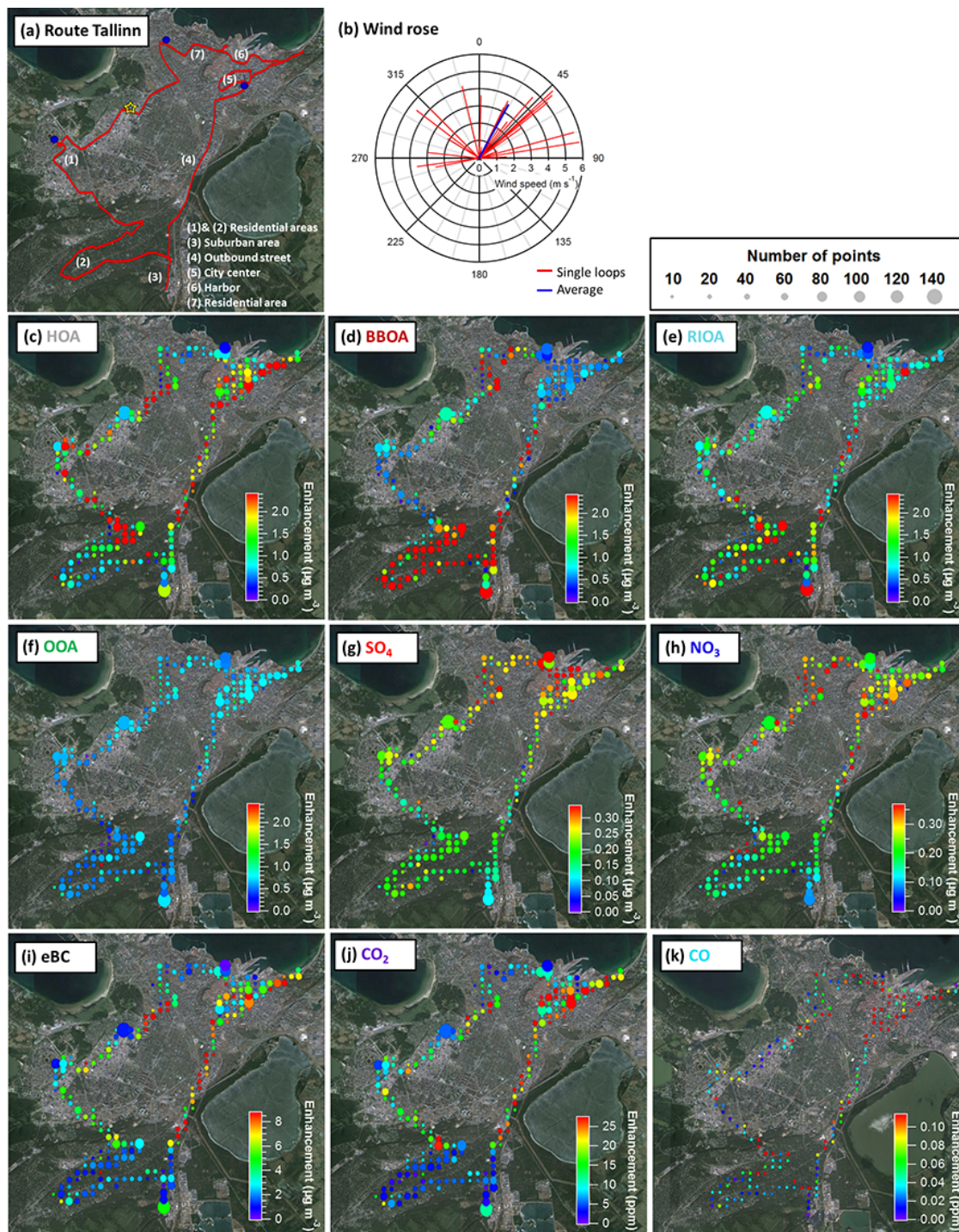


**Figure 5.** (a) Driving route in Tallinn: the red trace represents the GPS data, the yellow star the stationary measurements location, and the blue dots the monitoring stations of the Estonian Environmental Research Institute (EERC); (b) wind conditions during the mobile measurements in Tallinn: red traces represent the wind direction and speed for the single loops and the average of all loops is represented in blue; (c to k) average spatial distributions of all identified OA sources (panels c to f) and other measured components (panels g to k) in Tallinn. The color scales represent enhancement over the background concentrations; the maxima of the color scales have been fixed to the 75th percentile of the average enhancement of each component in panels (g) to (k) and to the highest 75th percentile among all OA sources in panels (c) to (f). The sizes of the points represent the number of points that have been averaged in each case (note: less data available for CO).

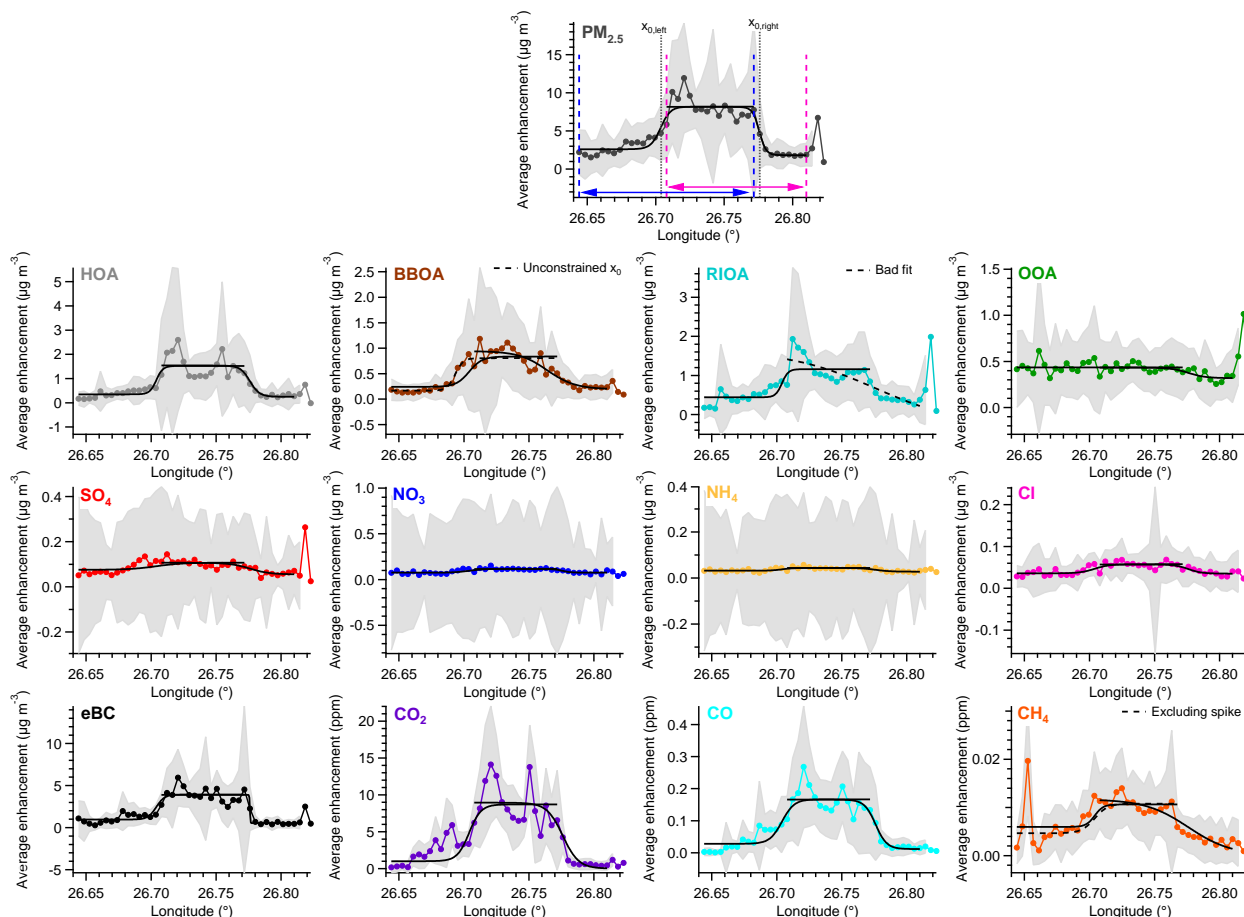


**Figure 6.** Average longitude profiles of the enhancements of all measured components and sources in Tartu. Colored curves represent the average enhancement of each source/components over 26 loops and the grey shaded area is the standard deviation among them. The average enhancements were fitted with sigmoid functions (black curves). The fitting limits (pink and blue arrows in top panel) and the sigmoid's midpoint ( $X_0$ ) were determined from the fit of the total  $\text{PM}_{2.5}$  mass (NR- $\text{PM}_{2.5}$  plus eBC) and then imposed to the other components/sources. Dashed black lines indicate a non-standard or bad fit (described in each case in the plot) and the results of these fits are represented in parentheses in Table 2. Notes: the spike found in the east for RIOA, OOA, and  $\text{SO}_4$  is not representative, as it is related to one single measurement point. The spike in  $\text{CH}_4$  in the west side is related to consistent increases of this component nearby a cowshed and will be further investigated in a future publication.

enhancement of  $0.8 \mu\text{g m}^{-3}$ ), these increases are negligible within the measurement and source apportionment uncertainties.

As reported in Table 3, the  $\text{PM}_{2.5}$  mass concentration in Tartu shows an urban increment of  $6.0 (4.6) \mu\text{g m}^{-3}$  over a regional background concentration of  $4.0 (3.5) \mu\text{g m}^{-3}$ . This leads to urban  $\text{PM}_{2.5}$  mass concentrations of up to  $10 (8.1) \mu\text{g m}^{-3}$ , which represents an increase of a factor 2.5 (2.3) in the particle mass concentration in the urban area compared to the regional background. About half of this enhancement is related to the emissions of eBC, which shows an increase of  $3.2 (2.3) \mu\text{g m}^{-3}$  over a regional background of  $1.1 (0.58) \mu\text{g m}^{-3}$ . Thus, the urban concentration of eBC is  $4.2 (2.9) \mu\text{g m}^{-3}$ , which represents an enhancement of a factor 3.9 (5.0) of eBC in the urban area. The primary OA sources explain a great part of the remaining increase in the

$\text{PM}_{2.5}$  mass: HOA is increased by a factor 3.6 (3.0) in the urban area and has a contribution of  $1.7 (1.0) \mu\text{g m}^{-3}$  to the urban concentration; RIOA is enhanced by a factor 2.0 (2.3), contributing  $1.7 (1.0) \mu\text{g m}^{-3}$  to the urban concentration; and BBOA is enhanced by a factor 3.1 (2.4) and contributes with  $1.0 (0.52) \mu\text{g m}^{-3}$  to the urban concentrations. In contrast, OOA and the inorganic species ( $\text{SO}_4$ ,  $\text{NO}_3$ ,  $\text{NH}_4$ , and Cl) show very low increases in the urban area, resulting in a total urban increment below  $0.21 \mu\text{g m}^{-3}$  (average and median). In the gas phase,  $\text{CO}_2$  shows an increase of  $8.3 (5.3) \text{ ppm}$  over a regional background of  $403.5 \text{ ppm}$  (both average and median); CO is increased by  $0.15 (0.11) \text{ ppm}$  over a regional background of  $0.16 (0.14) \text{ ppm}$ , which represents an increase of a factor 1.9 (1.7); while  $\text{CH}_4$  shows very similar concentrations inside and outside the city, with average (and me-

**Table 3.** Results obtained from the average (a) and median (b) longitude profiles for each measured component/source. P05 represents the averaged fifth percentile subtracted for the calculation of the enhancements; base and increment values were obtained from the sigmoid fits; the regional background is given as the sum of P05 and the average base value; urban concentrations are the sum of the regional background and the average urban increment; the factor increase represents the ratio between the urban and the regional backgrounds. Values in parentheses represent non-standard or bad fits and were not used in the calculations.

(a) Average longitude profiles										
	P05 <sup>a</sup>	Base			Urban increment			Regional background	Urban concentration	Factor increase
		west	east	average	west	east	average			
PM <sub>2.5</sub> (μg m <sup>−3</sup> )	1.8	2.6	1.8	2.2	5.6	6.3	6.0	4.0	10.0	2.5
HOA (μg m <sup>−3</sup> )	0.18	0.34	0.24	0.29	1.2	1.3	1.2	0.47	1.7	3.6
BBOA <sup>b</sup> (μg m <sup>−3</sup> )	0.11	0.24 (0.16)	0.19	0.21	0.60 (0.64)	0.75	0.67	0.32	1.0	3.1
RIOA (μg m <sup>−3</sup> )	0.27	0.44	(−0.30)	0.44	0.72	(1.9)	0.72	0.71	1.4	2.0
OOA (μg m <sup>−3</sup> )	0.44	0.42	0.32	0.37	0.024	0.11	0.069	0.81	0.87	1.1
SO <sub>4</sub> (μg m <sup>−3</sup> )	0.29	0.075	0.055	0.065	0.032	0.051	0.042	0.35	0.39	1.1
NO <sub>3</sub> (μg m <sup>−3</sup> )	0.095	0.075	0.076	0.075	0.042	0.038	0.040	0.17	0.21	1.2
NH <sub>4</sub> (μg m <sup>−3</sup> )	0.079	0.032	0.028	0.030	0.012	0.016	0.014	0.11	0.12	1.1
Cl (μg m <sup>−3</sup> )	0.012	0.036	0.035	0.035	0.022	0.022	0.022	0.047	0.069	1.5
eBC (μg m <sup>−3</sup> )	0.34	0.96	0.54	0.75	3.0	3.3	3.2	1.1	4.2	3.9
CO <sub>2</sub> (ppm)	403.0	0.99	0.04	0.52	7.8	8.9	8.3	403.5	411.9	1.0
CO (ppm)	0.14	0.028	0.012	0.020	0.14	0.15	0.15	0.16	0.31	1.9
CH <sub>4</sub> <sup>c</sup> (ppm)	1.90	0.0060 (0.0052)	< 0.001	0.0012	0.0047 (0.0064)	0.012	0.0083	1.90	1.91	1.0

(b) Median longitude profiles										
	P05 <sup>a</sup>	Base			Urban increment			Regional background	Urban concentration	Factor increase
		west	east	average	west	east	average			
PM <sub>2.5</sub> (μg m <sup>−3</sup> )	1.8	1.8	1.6	1.7	4.6	4.6	4.6	3.5	8.1	2.3
HOA (μg m <sup>−3</sup> )	0.18	0.16	0.13	0.14	0.66	0.66	0.66	0.33	1.0	3.0
BBOA (μg m <sup>−3</sup> )	0.11	0.088	0.12	0.11	0.35	0.27	0.31	0.22	0.52	2.4
RIOA (μg m <sup>−3</sup> )	0.27	0.20	0.15	0.17	0.58	0.60	0.59	0.45	1.0	2.3
OOA (μg m <sup>−3</sup> )	0.44	0.28	0.26	0.27	0.084	0.096	0.090	0.71	0.80	1.1
SO <sub>4</sub> (μg m <sup>−3</sup> )	0.29	0.064	0.053	0.059	0.029	0.039	0.034	0.35	0.38	1.1
NO <sub>3</sub> (μg m <sup>−3</sup> )	0.095	0.043	0.053	0.048	0.056	0.039	0.047	0.14	0.19	1.3
NH <sub>4</sub> (μg m <sup>−3</sup> )	0.079	0.028	0.026	0.027	0.0094	0.011	0.010	0.11	0.12	1.1
Cl (μg m <sup>−3</sup> )	0.012	0.022	0.025	0.024	0.024	0.019	0.021	0.035	0.06	1.6
eBC (μg m <sup>−3</sup> )	0.34	0.45	0.027	0.24	2.0	2.5	2.3	0.58	2.9	5.0
CO <sub>2</sub> (ppm)	403.0	0.95	0.051	0.50	5.0	5.6	5.3	403.5	408.8	1.0
CO (ppm)	0.14	0.011	< 0.001	0.0052	0.096	0.12	0.11	0.14	0.25	1.7
CH <sub>4</sub> <sup>c</sup> (ppm)	1.90	0.0032 (0.0028)	< 0.001	< 0.001	0.0051 (0.0055)	0.011	0.0079	1.90	1.91	1.0

<sup>a</sup> Excluding special events. <sup>b</sup> ( $X_0$  not fixed). <sup>c</sup> Excluding spike.

dian) regional background of 1.90 ppm and urban concentrations of 1.91 ppm.

Similar results were obtained for Tallinn (see Figs. 5 and S11). However, given the larger extension of this city, it was not possible to include a real regional background site in the route. Therefore, the longitude profiles and urban increments could not be properly explored for Tallinn. However, different source regions can still be distinguished within the examined area. Thus, the spatial distribution of HOA (Fig. 5c) is in agreement with those of eBC, CO<sub>2</sub>, and CO (Fig. 5i–k) and shows substantial increases in areas with high traffic and on major streets in the city center with significant stop-and-go

conditions. BBOA (Fig. 5d) has higher contributions in the residential areas, especially in region 2 of the driving route, where there is a very high density of residential wood combustion sources (see Fig. S1). Compared to Tartu, in Tallinn the spatial distribution of RIOA (Fig. 5e) is more homogeneous, with only slight enhancements in the residential area and in the city center. Finally, OOA (Fig. 5f) exhibits a small enhancement in the city center area, which again coincides with small increases in the secondary inorganic species concentrations (see Figs. 5g–h and S11) that are insignificant within the measurement and source apportionment uncertainties. Enhanced SO<sub>4</sub> levels are also found in the northern



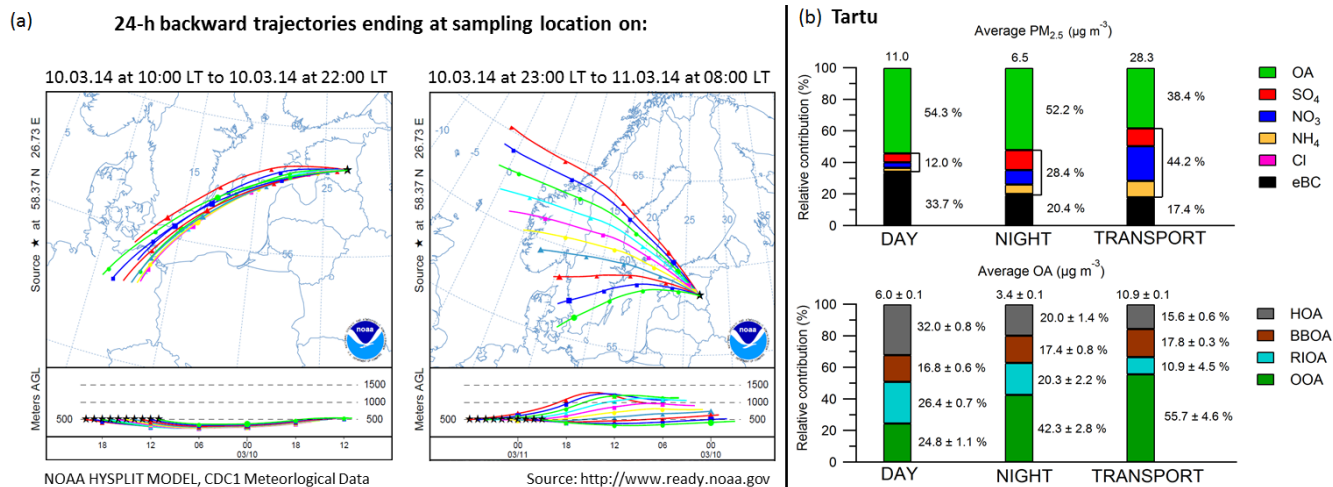


**Figure 7.** (a) 24 h back trajectories (NOAA HYSPLIT MODEL) of the air masses ending at the sampling location (Tartu) during the transport event (10 March between 10:00 and 22:00 LT, left panel) and the successive hours (from 10 March at 23:00 LT until 11 March at 08:00 LT, right panel). (b)  $PM_{2.5}$  mass concentration and chemical composition (top panel) and OA mass concentration and relative contributions of the OA sources (bottom panel) during the measurements in Tartu during daytime, nighttime, and transport event. Errors indicate the standard deviation among 100 bootstrap runs.

part of the route, likely from local ship emissions (Lack et al., 2009). Winds from the west and east were observed during the mobile measurements in Tallinn (Fig. 5b). In order to identify possible processes influencing the spatial distributions of the measured pollutants for the two different wind patterns, the average spatial distributions were calculated for all loops with western wind (7 loops) and loops with eastern wind (16 loops, excluding drives during accumulation events). The results of these analyses are reported in the supplementary information (Figs. S14 and S15) and show that, in general, the wind direction did not have an effect on the identified source areas and similar enhancements were found for both types of winds. A detailed analysis of these spatial distributions shows that BBOA,  $SO_4$ , and  $NO_3$  are more strongly enhanced during western winds, while HOA is more enhanced for eastern wind conditions. This difference is most probably related to the presence of western winds during the weekend (enhanced residential emissions) and eastern winds during the weekday measurements (enhanced traffic emissions).

### 3.4 Special events: transport and accumulation of pollutants

Enhanced concentrations of secondary species including OOA,  $SO_4$ ,  $NO_3$ , and  $NH_4$  were measured during the first measurement day in Tartu (see Figs. 1a and 3a). The analysis of the 24 h back trajectories reported in Fig. 7a indicates that these mostly secondary components were probably transported from continental Europe, in particular from northern Germany. The later decrease in the concentrations of these species coincides with clean air masses originating

from the Northern Atlantic at higher altitudes above ground level. As reported in Fig. 7b, during this transport event the average  $PM_{2.5}$  mass concentration increased to  $28.3 \mu g m^{-3}$  (compared to average concentrations of  $11.0 \mu g m^{-3}$  measured during daytime and  $6.5 \mu g m^{-3}$  during nighttime). This increase in mass is mostly related to the increased concentrations of the secondary components, especially of  $NO_3$  and OOA. Accordingly, the relative contributions of the inorganic species to the total NR- $PM_{2.5}$  increased to over 44 % during the transport event (compared to 12 % for daytime and around 28 % for nighttime averages) and the relative contribution of the OOA to total OA increased to 56 % (compared to 25 % for daytime and 42 % for nighttime averages). It is worthwhile to note that the source separation is more uncertain during the transport event due to lower statistics and increased mixing (if the transported air contains multiple sources). This is especially the case for RIOA, which has a relative error of 41 % (estimated by the bootstrapping procedure) during the transport event.

During the nights of 28 and 29 March, very high concentrations of organics (exceeding  $200 \mu g m^{-3}$ ), eBC (above  $15 \mu g m^{-3}$ ) and  $CO_2$  (up to 500 ppm) were measured in Tallinn, as shown in Fig. 8a. Relatively short back trajectories originating from the Baltic Sea (northwest and west of the sampling site) and at high altitudes were obtained for these periods (not reported). Moreover, as shown in Fig. 8a, during such accumulation events wind speed was close to zero and a strong near-ground temperature inversion (i.e., a positive temperature difference between the ground and 22 m a.g.l.) was observed. Under such conditions, the vertical mixing is suppressed and the local pollutants are trapped at the surface. As reported in Fig. 8b, during the accumulation periods the

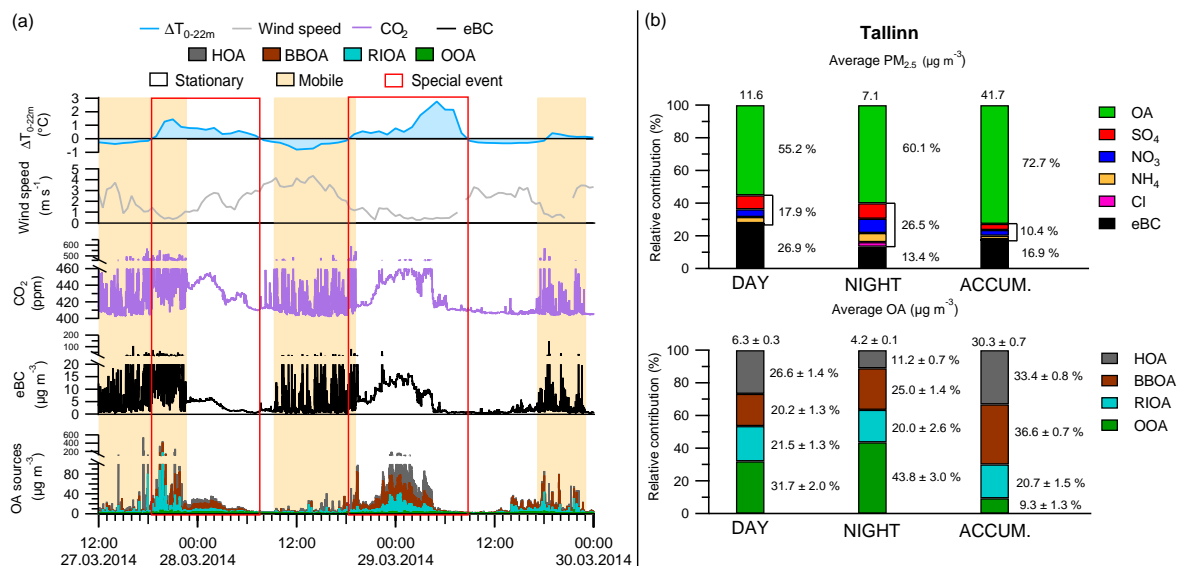


**Figure 8.** (a) Temporal evolution of the OA sources, eBC and CO<sub>2</sub>, wind speed, and  $\Delta T_{0-22m}$  (temperature difference between ground level and at 22 m above ground level) during the accumulation events in Tallinn. (b) PM<sub>2.5</sub> mass concentration and chemical composition (top panel) and OA mass concentration and relative contributions of the OA sources (bottom panel) during the measurements in Tallinn during daytime, nighttime, and accumulation events. Errors indicate the standard deviation among 100 bootstrap runs.

average PM<sub>2.5</sub> mass increased up to 41.7 μg m<sup>-3</sup>, with OA explaining 73 % of the total mass. This increase was mostly related to the increase of the primary aerosols, mainly HOA and BBOA, which explained 33 and 37 % of the OA mass, respectively.

## 4 Conclusions

Mobile measurements allowed for the study of the spatial distributions of major gas- and particle-phase pollutants in two urban areas in Estonia, permitting the identification of particular source areas and the determination of regional background concentrations and urban increments for the individual components/sources. A comprehensive set of instruments including a HR-ToF-AMS (with a newly developed inlet to measure the NR-PM<sub>2.5</sub> fraction), a seven-wavelength Aethalometer and several gas-phase monitors were deployed in the mobile laboratory to retrieve a detailed chemical characterization of the PM<sub>2.5</sub> fraction and the concentrations of several trace gases with high time resolution.

The measurements were performed in March 2014 in the two major cities of Estonia (Tallinn and Tartu) and no major differences were found in the chemical composition at the two sites. Higher mass concentrations were always measured during daytime, when point sources were sampled during mobile measurements. Under regular meteorological conditions, OA represented the largest mass fraction (on average 52.2 to 60.1 % of PM<sub>2.5</sub>), while the relative contribution of the inorganic species (mostly SO<sub>4</sub>, NO<sub>3</sub>, and NH<sub>4</sub>) strongly increased during the transport of polluted air masses from

northern Germany. Four sources of OA were identified by means of PMF: three primary sources (HOA, BBOA, and RIOA) and a secondary OA (OOA). Although the RIOA is thought to be dominated by cooking emissions, contributions from other residential emissions to this factor cannot be excluded. For example, waste burning is known to be a common process in some cities in Estonia (Maasikmets et al., 2015). However, to properly separate the contribution of waste burning from other co-emitting sources, laboratory studies of direct emissions need to be performed in the future. While OOA dominated the OA mass during nighttime (on average 42.3 % in Tartu and 43.8 % in Tallinn), the primary sources explained the major fraction of OA during daytime (75.2 % in Tartu and 68.3 % in Tallinn, with similar contributions from the three sources). During the period with transport of polluted air masses aforementioned, the OOA relative contribution was enhanced. In contrast, HOA, RIOA, and BBOA were strongly enhanced during periods characterized by temperature inversions, which induced the accumulation of locally emitted primary pollutants (primary OA and eBC).

Different source regions were identified inside the two urban areas. All traffic related pollutants (including HOA, eBC, CO<sub>2</sub>, and CO) were strongly enhanced on the major city roads, especially in areas with stop-and-go conditions during the morning and evening rush hours. BBOA showed a clear increase in the residential areas during the evening hours (due to domestic heating), while RIOA (believed to be strongly influenced by cooking emissions) was enhanced in both the city center (from restaurant cooking emissions) and in the residential areas (from domestic cooking). In contrast,



the secondary components (including OOA, SO<sub>4</sub>, NO<sub>3</sub>, NH<sub>4</sub>, and Cl) had very homogeneous spatial distributions, with no clear enhancement in the urban areas (within the measurement uncertainties) or at certain times of the day. For Tartu, regional background concentrations and urban increments of all measured components/sources were also determined. On average, the PM<sub>2.5</sub> mass had an enhancement inside the city of 6.0 µg m<sup>-3</sup> over the regional background concentration of 4.0 µg m<sup>-3</sup>. This urban increment was strongly related to the enhancement of eBC (3.2 µg m<sup>-3</sup>) and the primary OA sources (on average 1.2 µg m<sup>-3</sup> from HOA, 0.67 µg m<sup>-3</sup> from BBOA and 0.72 µg m<sup>-3</sup> from RIOA), while the secondary components (OOA, SO<sub>4</sub>, NO<sub>3</sub>, NH<sub>4</sub>, and Cl) did not contribute to a substantial enhancement. Moreover, the good correlation found between eBC with HOA indicates that up to 74 % of the enhancement in the PM<sub>2.5</sub> is related to traffic emissions in the urban area. CO<sub>2</sub> and CO, which were also found to be strongly correlated with HOA, had an average urban increment of 8.3 and 0.15 ppm over regional background concentrations of 403.5 and 0.15 ppm, respectively.

Our results show that mobile measurements are a very powerful technique for spatial characterization of the major pollutants in urban areas. The methodology presented in this work can be generalized to other cities in order to determine the influence of human activity on the particle sources and levels in different areas of a city and the related health effects.

**The Supplement related to this article is available online at doi:10.5194/acp-16-7117-2016-supplement.**

**Acknowledgements.** This work was carried out in the framework of the public procurement “Determination of Chemical Composition of Atmospheric Gases and Aerosols in Estonia” of the Estonian Environmental Research Centre (Reference number: 146623), funded by the Estonian–Swiss cooperation program “Enforcement of the surveillance network of the Estonian air quality: Determination of origin of fine particles in Estonia”. Jay G. Slowik acknowledges the support of the Swiss National Science Foundation (starting grant no. BSSGI0 155846). Imad El-Haddad acknowledges the support of the Swiss National Science Foundation (IZERZ0 142146). The authors gratefully acknowledge the NOAA Air Resources Laboratory (ARL) for the provision of the HYSPLIT transport and dispersion model and READY website (<http://www.ready.noaa.gov>) used in this publication.

Edited by: J. Surratt

## References

- Aiken, A. C., Salcedo, D., Cubison, M. J., Huffman, J. A., DeCarlo, P. F., Ulbrich, I. M., Docherty, K. S., Sueper, D., Kimmel, J. R., Worsnop, D. R., Trimborn, A., Northway, M., Stone, E. A., Schauer, J. J., Volkamer, R. M., Fortner, E., de Foy, B., Wang, J., Laskin, A., Shutthanandan, V., Zheng, J., Zhang, R., Gaffney, J., Marley, N. A., Paredes-Miranda, G., Arnott, W. P., Molina, L. T., Sosa, G., and Jimenez, J. L.: Mexico City aerosol analysis during MILAGRO using high resolution aerosol mass spectrometry at the urban supersite (T0) – Part 1: Fine particle composition and organic source apportionment, *Atmos. Chem. Phys.*, 9, 6633–6653, doi:10.5194/acp-9-6633-2009, 2009.
- Alfarra, M. R., Prévôt, A. S. H., Szidat, S., Sandradewi, J., Weimer, S., Lanz, V. A., Schreiber, D., Mohr, M., and Baltensperger, U.: Identification of the mass spectral signature of organic aerosols from wood burning emissions, *Environ. Sci. Technol.*, 41, 5770–5777, 2007.
- Allan, J. D., Delia, A. E., Coe, H., Bower, K. N., Alfarra, M. R., Jimenez, J. L., Middlebrook, A. M., Drewnick, F., Onasch, T. B., Canagaratna, M. R., Jayne, J. T., and Worsnop, D. R.: A generalized method for the extraction of chemically resolved mass spectra from Aerodyne aerosol mass spectrometer data, *J. Aerosol Sci.*, 35, 909–922, 2004.
- Ångström, A.: On the atmospheric transmission of sun radiation and on dust in the air, *Geogr. Ann.*, 11, 156–166, 1929.
- Baker, J.: A cluster analysis of long range air transport pathways and associated pollutant concentrations within the UK, *Atmos. Environ.*, 44, 563–571, 2010.
- Beekmann, M., Prévôt, A. S. H., Drewnick, F., Sciare, J., Pandis, S. N., Denier van der Gon, H. A. C., Crippa, M., Freutel, F., Poulain, L., Ghersi, V., Rodriguez, E., Beirle, S., Zotter, P., von der Weiden-Reinmüller, S.-L., Bressi, M., Fountoukis, C., Petetin, H., Szidat, S., Schneider, J., Rosso, A., El Haddad, I., Megaritis, A., Zhang, Q. J., Michoud, V., Slowik, J. G., Moukhtar, S., Kolmonen, P., Stohl, A., Eckhardt, S., Borbon, A., Gros, V., Marchand, N., Jaffrezo, J. L., Schwarzenboeck, A., Colomb, A., Wiedensohler, A., Borrmann, S., Lawrence, M., Baklanov, A., and Baltensperger, U.: In situ, satellite measurement and model evidence on the dominant regional contribution to fine particulate matter levels in the Paris megacity, *Atmos. Chem. Phys.*, 15, 9577–9591, doi:10.5194/acp-15-9577-2015, 2015.
- Bukowiecki, N., Dommen, J., Prévôt, A. S. H., Richter, R., Weingartner, E., and Baltensperger, U.: A mobile pollutant measurement laboratory: measuring gas phase and aerosol ambient concentrations with high spatial and temporal resolution, *Atmos. Environ.*, 36, 5569–5579, 2002.
- Bukowiecki, N., Dommen, J., Prévôt, A. S. H., Weingartner, E., and Baltensperger, U.: Fine and ultrafine particles in the Zürich (Switzerland) area measured with a mobile laboratory: an assessment of the seasonal and regional variation throughout a year, *Atmos. Chem. Phys.*, 3, 1477–1494, doi:10.5194/acp-3-1477-2003, 2003.
- Canonaco, F., Crippa, M., Slowik, J. G., Baltensperger, U., and Prévôt, A. S. H.: SoFi, an IGOR-based interface for the efficient use of the generalized multilinear engine (ME-2) for the source apportionment: ME-2 application to aerosol mass spectrometer data, *Atmos. Meas. Tech.*, 6, 3649–3661, doi:10.5194/amt-6-3649-2013, 2013.

- Carbone, C., Decesari, S., Mircea, M., Giulianelli, L., Finessi, E., Rinaldi, M., Fuzzi, S., Marinoni, A., Duchi, R., Perrino, C., Sargolini, T., Vardè, M., Sprovieri, F., Gobbi, G. P., Angelini, F., and Facchini, M. C.: Size-resolved aerosol chemical composition over the Italian Peninsula during typical summer and winter conditions, *Atmos. Environ.*, 44, 5269–5278, 2010.
- Crilley, L. R., Bloss, W. J., Yin, J., Beddows, D. C. S., Harrison, R. M., Allan, J. D., Young, D. E., Flynn, M., Williams, P., Zotter, P., Prevot, A. S. H., Heal, M. R., Barlow, J. F., Halios, C. H., Lee, J. D., Szidat, S., and Mohr, C.: Sources and contributions of wood smoke during winter in London: assessing local and regional influences, *Atmos. Chem. Phys.*, 15, 3149–3171, doi:10.5194/acp-15-3149-2015, 2015.
- Crippa, M., DeCarlo, P. F., Slowik, J. G., Mohr, C., Heringa, M. F., Chirico, R., Poulain, L., Freutel, F., Sciare, J., Cozic, J., Di Marco, C. F., Elsasser, M., Nicolas, J. B., Marchand, N., Abidi, E., Wiedensohler, A., Drewnick, F., Schneider, J., Borrmann, S., Nemitz, E., Zimmermann, R., Jaffrezo, J.-L., Prévôt, A. S. H., and Baltensperger, U.: Wintertime aerosol chemical composition and source apportionment of the organic fraction in the metropolitan area of Paris, *Atmos. Chem. Phys.*, 13, 961–981, doi:10.5194/acp-13-961-2013, 2013a.
- Crippa, M., El Haddad, I., Slowik, J. G., DeCarlo, P. F., Mohr, C., Heringa, M. F., Chirico, R., Marchand, N., Sciare, J., Baltensperger, U., and Prévôt, A. S. H.: Identification of marine and continental aerosol sources in Paris using high resolution aerosol mass spectrometry, *J. Geophys. Res.*, 118, 1950–1963, 2013b.
- DeCarlo, P. F., Kimmel, J. R., Trimborn, A., Northway, M. J., Jayne, J. T., Aiken, A. C., Gonin, M., Fuhrer, K., Horvath, T., Docherty, K. S., Worsnop, D. R., and Jimenez, J. L.: Field-deployable, high-resolution, time-of-flight aerosol mass spectrometer, *Anal. Chem.*, 78, 8281–8289, 2006.
- Di Gilio, A., de Gennaro, G., Dambruoso, P., and Ventrellaa, G.: An integrated approach using high time-resolved tools to study the origin of aerosols, *Sci. Total Environ.*, 530–531, 28–37, 2015.
- Dockery, D. W., Pope, C. A., Xu, X., Spengler, J. D., Ware, J. H., Fay, M. E., Ferris Jr., B. G., and Speizer, F. E.: An association between air pollution and mortality in six U.S. cities, *N. Engl. J. Med.*, 329, 1753–1759, 1993.
- Drinovec, L., Mocnik, G., Zotter, P., Prévôt, A. S. H., Ruckstuhl, C., Coz, E., Rupakheti, M., Sciare, J., Müller, T., Wiedensohler, A., and Hansen, A. D. A.: The “dual-spot” Aethalometer: an improved measurement of aerosol black carbon with real-time loading compensation, *Atmos. Meas. Tech.*, 8, 1965–1979, doi:10.5194/amt-8-1965-2015, 2015.
- El Haddad, I., D’Anna, B., Temime-Roussel, B., Nicolas, M., Bo-reave, A., Favez, O., Voisin, D., Sciare, J., George, C., Jaffrezo, J.-L., Wortham, H., and Marchand, N.: Towards a better understanding of the origins, chemical composition and aging of oxygenated organic aerosols: case study of a Mediterranean industrialized environment, Marseille, *Atmos. Chem. Phys.*, 13, 7875–7894, doi:10.5194/acp-13-7875-2013, 2013.
- Elser, M., Huang, R.-J., Wolf, R., Slowik, J. G., Wang, Q., Canonaco, F., Li, G., Bozzetti, C., Daellenbach, K. R., Huang, Y., Zhang, R., Li, Z., Cao, J., Baltensperger, U., El-Haddad, I., and Prévôt, A. S. H.: New insights into PM<sub>2.5</sub> chemical composition and sources in two major cities in China during extreme haze events using aerosol mass spectrometry, *Atmos. Chem. Phys.*, 16, 3207–3225, doi:10.5194/acp-16-3207-2016, 2016.
- Favez, O., El Haddad, I., Piot, C., Bor’ave, A., Abidi, E., Marchand, N., Jaffrezo, J.-L., Besombes, J.-L., Personnaz, M.-B., Sciare, J., Wortham, H., George, C., and D’Anna, B.: Inter-comparison of source apportionment models for the estimation of wood burning aerosols during wintertime in an Alpine city (Grenoble, France), *Atmos. Chem. Phys.*, 10, 5295–5314, doi:10.5194/acp-10-5295-2010, 2010.
- Gao, M., Guttikunda, S. K., Carmichael, G. R., Wang, Y., Liu, Z., Stanier, C. O., Saide, P. E., and Yu, M.: Health impacts and economic losses assessment of the 2013 severe haze event in Beijing area, *Sci. Total Environ.*, 511, 553–561, 2015.
- Herich, H., Hueglin, C., and Buchmann, B.: A 2.5 year’s source apportionment study of black carbon from wood burning and fossil fuel combustion at urban and rural sites in Switzerland, *Atmos. Meas. Tech.*, 4, 1409–1420, doi:10.5194/amt-4-1409-2011, 2011.
- Hu, D. and Jiang, J.: PM<sub>2.5</sub> pollution and risk for lung cancer: A rising issue in China, *J. Environ. Prot.*, 5, 731–738, 2014.
- Kwak, J. H., Kim, H. S., Lee, J. H., and Lee, S. H.: On-road chasing measurement of exhaust of particle emissions from diesel, CNG LPG and DME-fueled vehicles using a mobile emission laboratory, *Int. J. Vehicle Des.*, 15, 543–551, 2014.
- Kyung Hwan, K., Daekwang, W., Seung-Bok, L., and Gwi-Nam, B.: On-road measurements of ultrafine particles and associated air pollutants in a densely populated area of Seoul, Korea, *Aerosol Air Qual. Res.*, 15, 142–153, 2015.
- Lack, D. A., Corbett, J. J., Onasch, T., Lerner, B., Massoli, P., Quinn, P. K., Bates, T. S., Covert, D. S., Coffman, D., Sierau, B., Herndon, S., Allan, J., Baynard, T., Lovejoy, E., Ravishankara, A. R., and Williams, E.: Particulate emissions from commercial shipping: Chemical, physical, and optical properties, *J. Geophys. Res.*, 114, D00F04, doi:10.1029/2008JD011300, 2009.
- Laden, F., Schwartz, J., Speizer, F. E., and Dockery, D. W.: Reduction in fine particulate air pollution and mortality: Extended follow-up of the Harvard Six Cities study, *Am. J. Respir. Crit. Care. Med.*, 173, 667–672, 2006.
- Lenschow, P., Abraham, H. J., Kutzner, K., Lutz, M., Preuß, J. D., and Reichenbacher, W.: Some ideas about the sources of PM<sub>10</sub>, *Atmos. Environ.*, 35, Supplement 1, S23–S33, 2001.
- Maasikmets, M., Kupri, H.-L., Teinmaa, E., Väinämäe, K., Arumäe, T., and Kimmel, V.: ACSM study to assess possible municipal solid waste burning in household stoves, Poster presented at: European Aerosol Conference 2015, Milan (Italy), 6–11 September 2015.
- Middlebrook, A. M., Bahreini, R., Jimenez, J. L., and Canagaratna, M. R.: Evaluation of composition-dependent collection efficiencies for the Aerodyne aerosol mass spectrometer using field data, *Aerosol Sci. Technol.*, 46, 258–271, 2012.
- Mohr, C., Richter, R., DeCarlo, P. F., Prévôt, A. S. H., and Baltensperger, U.: Spatial variation of chemical composition and sources of submicron aerosol in Zurich during wintertime using mobile aerosol mass spectrometer data, *Atmos. Chem. Phys.*, 11, 7465–7482, doi:10.5194/acp-11-7465-2011, 2011.
- Mohr, C., DeCarlo, P. F., Heringa, M. F., Chirico, R., Slowik, J. G., Richter, R., Reche, C., Alastuey, A., Querol, X., Seco, R., Peñuelas, J., Jimenez, J. L., Crippa, M., Zimmermann, R., Baltensperger, U., and Prévôt, A. S. H.: Identification and quantification of organic aerosol from cooking and other sources in

- Barcelona using aerosol mass spectrometer data, *Atmos. Chem. Phys.*, 12, 1649–1665, doi:10.5194/acp-12-1649-2012, 2012.
- Mohr, C., DeCarlo, P. F., Heringa, M. F., Chirico, R., Richter, R., Crippa, M., Querol, X., Baltensperger, U., and Prévôt, A. S. H.: Spatial variation of aerosol chemical composition and organic components identified by positive matrix factorization in the Barcelona region, *Environ. Sci. Technol.*, 49, 10421–10430, 2015.
- Myhre, G., Shindell, D., Bréon, F.-M., Collins, W., Fuglestad, J., Huang, J., Koch, D., Lamarque, J.-F., Lee, D., Mendoza, B., Nakajima, T., Robock, A., Stephens, G., Takemura, T., and Zhang, H.: Anthropogenic and Natural Radiative Forcing. In: *Climate Change 2013: The Physical Science Basis. Contribution of Working Group I to the Fifth Assessment Report of the Intergovernmental Panel on Climate Change*, edited by: Stocker, T. F., Qin, D., Plattner, G.-K., Tignor, M., Allen, S. K., Boschung, J., Nauels, A., Xia, Y., Bex, V., and Midgley, P. M., Cambridge University Press, Cambridge, United Kingdom and New York, NY, USA, 2013.
- Ng, N. L., Canagaratna, M. R., Jimenez, J. L., Zhang, Q., Ulbrich, I. M., and Worsnop, D. R.: Real-time methods for estimating organic component mass concentrations from aerosol mass spectrometer data, *Environ. Sci. Technol.*, 45, 910–916, 2011.
- Niemi, J. V., Saarikoski, S., Aurela, M., Tervahattu, H., Hillamo, R., Westphal, D. L., Aarnio, P., Koskentalo, T., Makkonen, U., Vehkamäki, H., and Kulmala, M.: Long-range transport episodes of fine particles in southern Finland during 1999–2007, *Atmos. Environ.*, 43, 1255–1264, 2009.
- Orru, H., Maasikmets, M., Lai, T., Tamm, T., Kaasik, M., Kimmel, V., Orru, K., Merisalu, E., and Forsberg, B.: Health impacts of particulate matter in five major Estonian towns: main sources of exposure and local differences, *Air Qual. Atmos. Health*, 4, 247–258, 2011.
- Paatero, P.: Least squares formulation of robust non-negative factor analysis, *Chemom. Intell. Lab. Syst.*, 37, 23–35, 1997.
- Paatero, P. and Hopke, P. K.: Discarding or downweighting high-noise variables in factor analytic models, *Anal. Chim. Acta*, 490, 277–289, 2003.
- Paatero, P. and Tapper, U.: Positive matrix factorization: a non-negative factor model with optimal utilization of error estimates of data values, *Environmetrics*, 5, 111–126, 1994.
- Paatero, P., Eberly, S., Brown, S. G., and Norris, G. A.: Methods for estimating uncertainty in factor analytic solutions, *Atmos. Meas. Tech.*, 7, 781–797, doi:10.5194/amt-7-781-2014, 2014.
- Pirjola, L., Parviainen, H., Hussein, T., Valli, A., Hämeri, K., Aalto, P., Virtanen, A., Keskinen, J., Pakkanen, T. A., Mäkelä, T., and Hillamo, R. E.: “Sniffer” – a novel tool for chasing vehicles and measuring traffic pollutants. *Atmos. Environ.*, 38, 3625–3635, 2004.
- Pirjola, L., Paasonen, P., Pfeiffer, D., Hussein, T., Hämeri, K., Koskentalo, T., Virtanen, A., Rönkkö, T., Keskinen, J., Pakkanen, T. A., and Hillamo, R. E.: Dispersion of particles and trace gases nearby a city highway: mobile laboratory measurements in Finland, *Atmos. Environ.*, 40, 867–879, 2006.
- Pirjola, L., Lähde, T., Niemi, J. V., Kousa, A., Rönkkö, T., Karjalainen, P., Keskinen, J., Frey, A., and Hillamo, R. E.: Spatial and temporal characterization of traffic emission in urban microenvironments with a mobile laboratory, *Atmos. Environ.*, 63, 156–167, 2012.
- Pirjola, L., Virkkula, A., Petaja, T., Levula, J., Kukkonen, J., and Kulmala, M.: Mobile ground-based measurements of aerosol and trace gases during a prescribed burning experiment in boreal forest in Finland, *Boreal Environ. Res.*, 20, 105–119, 2015.
- Pope, C. A. and Dockery, D. W.: Health effects of fine particulate air pollution: lines that connect, *J. Air Waste Manag. Assoc.*, 56, 709–742, 2006.
- Putaud, J. P., Raes, F., Van Dingenen, R., Brüggemann, E., Facchini, M. C., Decesari, S., Fuzzi, S., Gehrig, R., Hüglin, C., Laj, P., Lorbeer, G., Maenhaut, W., Mihalopoulos, N., Müller, K., Querol, X., Rodriguez, S., Schneider, J., Spindler, G., ten Brink, H., Tørseth, K., and Wiedensohler, A.: A European aerosol phenomenology – 2: chemical characteristics of particulate matter at kerbside, urban, rural and background sites in Europe, *Atmos. Environ.*, 38, 2579–2595, 2004.
- Putaud, J.-P., Van Dingenen, R., Alastuey, A., Bauer, H., Birmili, W., Cyrys, J., Flentje, H., Fuzzi, S., Gehrig, R., Hansson, H. C., Harrison, R. M., Herrmann, H., Hitznerberger, R., Hüglin, C., Jones, A. M., Kasper-Giebl, A., Kiss, G., Kousam, A., Kuhlbusch, T. A. J., Löschau, G., Maenhaut, W., Molnar, A., Moreno, T., Pekkanen, J., Perrino, C., Pitz, M., Puxbaum, H., Querol, X., Rodriguez, S., Salma, I., Schwarz, J., Smolik, J., Schneider, J., Spindler, G., ten Brink, H., Tursic, J., Viana, M., Wiedensohler, A., and Raes, F.: A European aerosol phenomenology – 3: Physical and chemical characteristics of particulate matter from 60 rural, urban, and kerbside sites across Europe, *Atmos. Environ.*, 44, 1308–1320, 2010.
- Ramanathan, V., Crutzen, P. J., Kiehl, J. T., and Rosenfeld, D.: Aerosols, climate, and the hydrological cycle, *Science*, 294, 2119–2124, 2001.
- Salvador, P., Artinano, B., Molero, F., Viana, M., Pey, J., Alastuey, A., and Querol, X.: African dust contribution to ambient aerosol levels across central Spain: Characterization of long-range transport episodes of desert dust, *Atmos. Res.*, 127, 117–129, 2013.
- Sandradewi, J., Prévôt, A. S. H., Szidat, S., Perron, N., Alfarra, M. R., Lanz, V. A., Weingartner, E., and Baltensperger, U.: Using aerosol light absorption measurements for the quantitative determination of wood burning and traffic emission contributions to particulate matter, *Environ. Sci. Technol.*, 42, 3316–3323, 2008.
- Sciare, J., d’Argouges, O., Sarda-Estève, R., Gaimoz, C., Dolgorouky, C., Bonnaire, N., Favez, O., Bonsang, B., and Gros, V.: Large contribution of water-insoluble secondary organic aerosols in the region of Paris (France) during wintertime, *J. Geophys. Res. Atmos.*, 116, D22203, doi:10.1029/2011JD015756, 2011.
- Setyan, A., Zhang, Q., Merkel, M., Knighton, W. B., Sun, Y., Song, C., Shilling, J. E., Onasch, T. B., Herndon, S. C., Worsnop, D. R., Fast, J. D., Zaveri, R. A., Berg, L. K., Wiedensohler, A., Flowers, B. A., Dubey, M. K., and Subramanian, R.: Characterization of submicron particles influenced by mixed biogenic and anthropogenic emissions using high-resolution aerosol mass spectrometry: results from CARES, *Atmos. Chem. Phys.*, 12, 8131–8156, doi:10.5194/acp-12-8131-2012, 2012.
- Squizzato, S., Masiol, M., Innocente, E., Pecorari, E., Rampazzo, G., and Pavoni, B.: A procedure to assess local and long-range transport contributions to PM<sub>2.5</sub> and secondary inorganic aerosol, *J. Aerosol Sci.*, 46, 64–76, 2012.
- Statistical database: Statistics Estonia, available at: <http://pub.stat.ee>, last access: 9 November 2015.

- Sun, Y.-L., Zhang, Q., Schwab, J. J., Demerjian, K. L., Chen, W.-N., Bae, M.-S., Hung, H.-M., Hogrefe, O., Frank, B., Rattigan, O. V., and Lin, Y.-C.: Characterization of the sources and processes of organic and inorganic aerosols in New York city with a high-resolution time-of-flight aerosol mass spectrometer, *Atmos. Chem. Phys.*, 11, 1581–1602, doi:10.5194/acp-11-1581-2011, 2011.
- Ulbrich, I. M., Canagaratna, M. R., Zhang, Q., Worsnop, D. R., and Jimenez, J. L.: Interpretation of organic components from Positive Matrix Factorization of aerosol mass spectrometric data, *Atmos. Chem. Phys.*, 9, 2891–2918, doi:10.5194/acp-9-2891-2009, 2009.
- Ulevicius, V., Bycenkiene, S., Bozzetti, C., Vlachou, A., Plauškaitė, K., Mordas, G., Dudoitis, V., Abbaszade, G., Remeikis, V., Garbaras, A., Masalaite, A., Blees, J., Fröhlich, R., Dällenbach, K. R., Canonaco, F., Slowik, J. G., Dommen, J., Zimmermann, R., Schnelle-Kreis, J., Salazar, G. A., Agrios, K., Szidat, S., El Haddad, I., and Prévôt, A. S. H.: Fossil and non-fossil source contributions to atmospheric carbonaceous aerosols during extreme spring grassland fires in Eastern Europe, *Atmos. Chem. Phys.*, 16, 5513–5529, doi:10.5194/acp-16-5513-2016, 2016.
- Urb, G., Teinemaa, E., Kettrup A., Gebefügi, I., Laja, M., Reinik, J., Tamm, E., and Kirso, U.: Atmospheric pollution in Tallinn, levels of priority pollutants, *Proc. Estonian Acad. Sci. Chem.*, 54, 123–133, 2005.
- von der Weiden-Reinmüller, S.-L., Drewnick, F., Crippa, M., Prévôt, A. S. H., Meleux, F., Baltensperger, U., Beekmann, M., and Borrmann, S.: Application of mobile aerosol and trace gas measurements for the investigation of megacity air pollution emissions: the Paris metropolitan area, *Atmos. Meas. Tech.*, 7, 279–299, doi:10.5194/amt-7-279-2014, 2014a.
- von der Weiden-Reinmüller, S.-L., Drewnick, F., Zhang, Q. J., Freutel, F., Beekmann, M., and Borrmann, S.: Megacity emission plume characteristics in summer and winter investigated by mobile aerosol and trace gas measurements: the Paris metropolitan area, *Atmos. Chem. Phys.*, 14, 12931–12950, doi:10.5194/acp-14-12931-2014, 2014b.
- Williams, L. R., Gonzalez, L. A., Peck, J., Trimborn, D., McInnis, J., Farrar, M. R., Moore, K. D., Jayne, J. T., Robinson, W. A., Lewis, D. K., Onasch, T. B., Canagaratna, M. R., Trimborn, A., Timko, M. T., Magoon, G., Deng, R., Tang, D., de la Rosa Blanco, E., Prévôt, A. S. H., Smith, K. A., and Worsnop, D. R.: Characterization of an aerodynamic lens for transmitting particles greater than 1 micrometer in diameter into the Aerodyne aerosol mass spectrometer, *Atmos. Meas. Tech.*, 6, 3271–3280, doi:10.5194/amt-6-3271-2013, 2013.
- Wolf, R., El Haddad, I., Crippa, M., Decesari, S., Slowik, J. G., Poulain, L., Gilardoni, S., Rinaldi, M., Carbone, S., Canonaco, F., Huang, R.-J., Baltensperger, U., and Prévôt, A. S. H.: Marine and urban influences on summertime PM<sub>2.5</sub> aerosol in the Po basin using mobile measurements, *Atmos. Environ.*, 120, 447–454, 2015.
- Zotter, P.: Sources of fossil and non-fossil atmospheric aerosols, PhD thesis, Eidgenössische Technische Hochschule, ETH Zürich, Switzerland, 2015.